Modeling the Effect of Flow-Induced Vibration on Submerged Structure

Muhammad Aqeel[1], Huabing Wen[1], Zhao Xianrui[1], Muhammad Shehryar Manzoor[2], Waqas Arif[2], Wei Wei[1]

[1]School of Naval Architecture & Intelligent Manufacturing, Jiangsu Maritime Institute, Nanjing, China. Zip Code: 211170

[2]Department of Mechanical Engineering Technology, National Skills University, Islamabad, Pakistan. Zip Code: 44000

Corresponding author: Muhammad Aqeel , Email: Muhammad.aqeel661@gmail.com

ABSTRACT

Flow-induced vibration (FIV) poses a critical risk of fatigue and failure to submerged structures like pipelines and marine energy devices; however, predictive modeling remains challenging due to a gap in integrated approaches that combine high-fidelity simulation with experimental validation across a broad parametric space. This study therefore aimed to quantify the effects of key geometric and hydrodynamic parameters on FIV response and to develop a validated predictive framework. A combined experimental-numerical methodology was employed, testing circular, square, and D-section models in a flume under systematically varied flow velocities and turbulence intensities. Data on structural displacement and hydrodynamic forces were collected using laser vibrometry, load cells, and PIV, alongside complementary fluid-structure interaction (FSI) simulations. A stratified sampling strategy generated 600 experimental runs and 120 simulations, with data analyzed via ANOVA, regression, and uncertainty quantification. Results demonstrated that cross-sectional geometry dominated the structural response. The square section exhibited the highest mean normalized RMS displacement (0.199 ± 0.061), significantly larger ($p < 0.001$) than the circular (0.118 ± 0.052) and D-sections (0.095 ± 0.038). A highly significant interaction ($p < 2e\text{-}16$) between reduced velocity and damping ratio governed the circular section's amplitude. Furthermore, increasing turbulence intensity from 5% to 15% significantly reduced the RMS lift coefficient ($p = 5.89e\text{-}7$). The research provides a robust, validated model that explicitly links flow conditions to structural response, offering engineers a critical tool for designing resilient submerged infrastructure against FIV.

Keywords: Flow-induced vibration, fluid-structure interaction, hydrodynamic loading, submerged structures, vortex-induced vibration.

INTRODUCTION

Flow-induced vibration (FIV) is an old phenomenon that has been considered crucial in designing and running any submerged structure when it is faced with fluidstructure interactions (Naqash & Alam, 2025). As a fluid goes over a bluff body or a structural object the successive shedding of vortices results in oscillating forces that can cause the structure to vibrate. Uncontrolled such vibrations can cause structural fatigue, resonance, and catastrophic failure, as found in pipelines, offshore platforms, bridge piers and marine energy equipment (Aqeel et al.,2025). This issue of forecasting and prevention of FIV has therefore become an urgent topic in fluid mechanics and structural engineering that requires a combination of experimental, numerical, and theoretical studies (Wu et al., 2022). This has been complicated by nonlinear interaction of the hydrodynamic forces and structural dynamics that depends on various parameters such as Reynolds number, reduced velocity, mass ratio, and damping (Ahmed, 2024; Filo et al., 2025). Although basic principles of vortex-driven vibration have been investigated in idealized situations, predictive models of FIV have not been fully developed under realistic submerged environment, especially when the laboratory results are scaled to full-sized engineering applications (Vaidya, 2025).

The present study is local and global in its scope as it indicates the relevance of submerged structures globally and their susceptibility to FIV. In river and coastal engineering projects, locally, submerged objects like the intake towers, pipelines and base of

the bridge are prone to disrupting currents, which may cause vibration and fatigue over a period of time (Stewart & Martin, 2021). FIV is an important design factor of risers, mooring systems, and underwater pipelines in countries that rely on offshore oil and gas exploitation e.g. in the Arabian Gulf and Southeast Asia. The growing use of renewable ocean energy systems worldwide such as tidal turbines, wave energy converters, and floating wind platforms has led to the concern of the urgent necessity to learn FIV over a wider typology of structural designs and flow-field conditions (Basha et al., 2021). The emergence of climate-related alterations, including increased hydrodynamic loading as a result of the increasing number of storms and stronger currents, enhances the need of sound predictive models even more (Burhanuddin et al., 2022). Thus, FIV is of not only theoretical interest but also of direct practical concern in regard to safety, lifespan, and functionality of submerged infrastructure across the globe.

The literature is very helpful in the comprehension of FIV, but it also unveils some gaps that inspire the current work. Earlier work, including that by Blevins and later Sarpkaya, developed basic paradigms of vortex-induced vibration in cylindrical structures. These models determined lock-in regimes, in which the vortex shedding frequency is in phase with natural frequency of the structure, and which increases the amplitude of the response (Boudina et al., 2021). Later studies developed these ideas by examining how response behavior depends on turbulence, scaling of Reynolds number, and added mass Khaled & Aly, , 2022). Computational fluid dynamics (CFD) and fluidstructure interaction (FSI) models have been adopted within the past decades in order to improve prediction of FIV (Aqeel et al.,2025). The challenges, however, remain in the capture of the nonlinearities of the flow conditions to real world conditions, such as turbulence spectra and three-dimensional wake interactions (Wu et al., 2022). Recent work has covered flexible and intricate geometries, and work has demonstrated that shape cross-sectional and structural damping has a very significant contribution to vibration properties. In spite of these developments, the number of predictive models that combine high-fidelity simulations with experimental validation is still sparse, especially in cases of submerged structures in combined flow regimes or in localized environmental conditions (Zhang et al., 2024).

This research has significance in that it could fill the gap between what is known and that which is practiced. FIV engineering breakdowns are well documented and some have resulted in expensive energy supply and transport hiccups (Aqeel et al.,2025).. An example can be given of subsea pipeline failures due to fatigue imposed on the pipeline by vibration and the consequences of this fatigue in terms of cost and safety of inadequate predictive capability (Rattansingh et al., 2024). Further, as renewable marine power infrastructure grows at an unprecedented pace, the response of submerged support structures to unsteady hydrodynamic forces is a central issue of infrastructure design (Sun et al., 2025). The study is therefore essential towards understanding science and engineering practice. The study is also valuable since it examines the vibration response under controlled laboratory and simulation environment in addition to establishing a modeling framework that can be applied to the real world (Kwak, 2022).

The need to carry out this research is precipitated by the combination of scientific interest and industrial imperative. Although a lot is known concerning canonical FIV scenarios, engineering structures are not idealized in terms of laboratory models (Papukchiev et al., 2024). Actual structures are faced with a broad spectrum of velocities, levels of turbulence, and geometrical intricacies. Moreover, directing laboratory data to field uses usually causes a mismatch, since the Reynolds numbers do not match and the environment is not consistent. The aim of this research was therefore to create quality data and predictive models that can bridging this gap (Eidi et al., 2022). The combination of laboratory experimentation, high-fidelity numerical modeling, and rigorous statistical analysis was aimed at generating a validated model that can predict vibration behavior within a reasonable degree of reliability that can be applied to engineering design imperatives (Ganguli, 2025).

The gap in research that is managed in this work is at the border of fluid and structural mechanics. Though past research has given an understanding on the mechanisms of the vortex shedding and lock-ins, most of them were limited to simplistic geometries or restricted sets of flow parameters. The absence of combined models that would take

into account simultaneously, geometric effects, turbulence spectra, mass-damping ratios and hydrodynamic coefficients, form a pronounced literature gap (Tang et al., 2025). In addition, the bulk of the literature focuses on experimental measurements or to a large extent, the literature is based on computational simulation, and only a few studies have tried to derive a mutual complementary manner between the two. The research will specifically fill this gap by creating a combined approach to experimental and computational processes with the help of statistical rigor to derive a generalizable result.

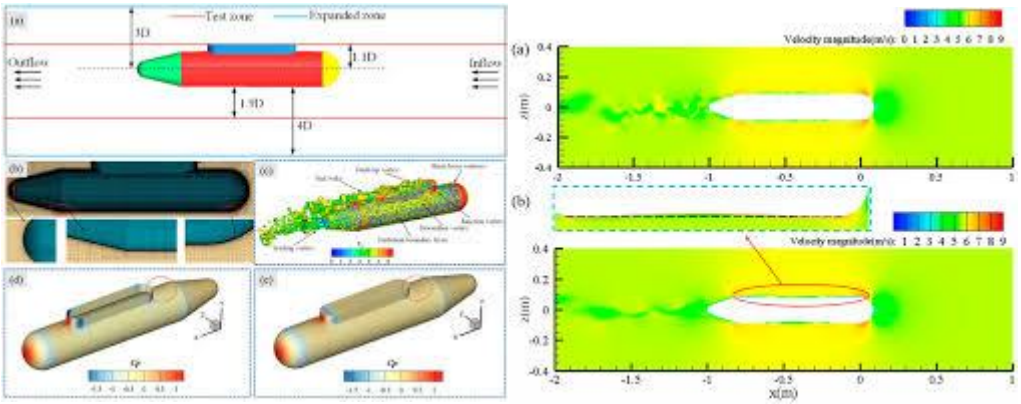

Figure 1: Study on Flow-Induced Vibration of Underwater Vehicle

The methodological research questions were formulated in accordance with this gap and to lead the study. Critical questions were: Which differences in the flow parameters (velocity, turbulence intensity) affect the amplitude and frequency of FIV in submerged structures? What influence geometric and structural properties, including cross-sectional shape and damping ratio, the hydrodynamic coefficients and overall vibration response? How far can the experimental observations be reproduced by a high-fidelity simulation and how can these be aggregated into an predictive modeling structure? These questions were used to narrow the scope of the experimental design, choice of parameters, and the approaches to analysis to make sure that each step of the research helps to answer both theoretical and practical issues.

In line with these questions, the objectives of the study were stated with direct reference to the methodology. The initial goal was to experimentally characterize the correlation between flow conditions and structural response over a broad parametric space and thus to provide ground-truth data to be validated. The second aim was to explore the geometry and damping effects in vibration response shaping with experimental and computational methods. The goal three was to model these results into an anticipatory modeling platform that can simulate FIV on submerged structures with an acceptable result. These aims led to the methodological decisions, including test condition selection, application of advanced techniques to measure flow, as well as use of CFD-based FSI simulators and statistical analyses and uncertainty analysis.

METHODOLOGY

The research problem stated above and to address the central research question: How do flow parameters and structural properties govern the amplitude, frequency content, and fatigue-relevant loading of submerged structures? three objectives were met. First, the relationship between flow conditions (velocity, turbulence intensity, spectral content) and structural response (displacement amplitude, dominant frequency, and damping) in a wide reduced-velocity range was quantified to determine regimes of lock-in and vortex-induced resonance. Second, it described the changes in hydrodynamic coefficients (drag, lift, added mass) and response spectra with geometric and structural parameters (cross-sectional shape, mass ratio, stiffness, and damping), providing physical mechanisms and response to observation. Third, it created and tested a predictive modeling framework integrating high-fidelity fluid-structure interaction (FSI) simulations and reduced-order surrogate models and uncertainty quantification to allow predicting the vibration amplitudes as well as

fatigue loading reliably to support engineering design. All of the objectives directly addressed the research problem and the research question as a whole by shifting between observation (objective 1) to mechanism (objective 2), and predictive capability (objective 3).

Research site

Experimental: experimental work had been conducted in the university fluid mechanics laboratory (hydraulics/flume facility) and structural dynamics workshop, and numerical simulation and post-processing had been conducted in the institutional high-performance computing cluster and desktop workstations using CFD/FEA software and MATLAB/Python toolchains.

2. Research design

Type of study

It involved a combined experimental-numerical (mixed-method) design that combined controlled laboratory experiments with complementary computational fluid-structure interaction (FSI) modelling. This mixed methodology was categorized as causal-experimental in the laboratory aspect (flow and structural parameter manipulation) and computational-modelling in the simulation aspect.

Research Design

Combined experimental-numerical design was the most suitable as experimental tests gave ground-truth measurements of FIV phenomena and calibration data, whereas high-fidelity simulations enabled systematic search of parameter space and went beyond practical experiment bounds. Experiments determined cause-and-effect relationships (e.g., between flow velocity and response amplitude) at controlled boundary conditions; simulations extrapolated those results to other geometries, flow regimes, and combinations of parameters, making it possible to validate and predict expertly.

Implementation example.

Single-degree-freedom and multi-degree-freedom submerged models were experimented in the flume under controlled single-degree-freedom and multi-degree-freedom conditions, with specified velocities and turbulence levels; parallel FSI simulations were used to replicate the experiments in order to allow direct validation and sensitivity analysis.

3. Study parameters

The essential parameters under which the study was governed were outlined and measured. Flow parameters included mean flow velocity (U, m/s), turbulence intensity (TI), integral length scale (L, m), and spectral properties (power spectral density). Structural parameters included natural frequencies (f n, Hz), modal damping ratios ( ), modal mass (m), stiffness (k), mass ratio (m = structure mass / displaced fluid mass), and geometry parameters (diameter/width/height, and surface roughness). Generalization numbers were non-dimensional Reynolds number (Re = U D/nu), Strouhal number (St =f s D / U), reduced velocity (U = / f n D), and Keulegan-Carpenter number (where applicable). Peak and RMS displacement (m), acceleration (m-s-2), force coefficients (C D, C L), and spectral characteristics (dominant frequency, bandwidth) were response metrics of interest.

4. Sampling strategy

Population and sample procedure

Population included test conditions parameterized by geometry (three canonical cross-sections: circular, rectangular, and rectangular with appendage), mass/damping parameters (low, medium, high mass ratio and damping) and flow states (a continuous range of mean velocities and three levels of turbulence intensity). The sampling of parameter space employed a stratified Latin-Hypercube scheme to evenly cover velocity, TI, and geometric parameters, and then higher concentration in the reduced-velocity range where lock-in was anticipated.

Justification and sample size

The experimental campaign consisted of thirty different physical test conditions (each run a total of 20 times to achieve statistical strength) which resulted in 600 experimental runs; the numerical campaign included approximately 120 validated FSI simulations selected by design-of-experiments (DOE) in the same parametric space. Experimental repetition (n 20 or more per condition) guaranteed dependable estimation of mean and variance of response measures (central limit theory) and detection of medium effects with conventional confidence (approximately 95 percent confidence).

The numerical sample size was determined to allow surrogate model training and cross-validation and to balance the computational cost.

Inclusion/exclusion criteria

There were also configurations built structurally stable under test conditions and which had been replicated typical submerged engineering elements. Conditions giving rise to flow conditions beyond facility capability (e.g., extremely high Froude/Reynolds number not possible in the flume), or conditions that threatened to destroy instrumentation were omitted.

5. Data collection methods

Instruments

Laser Doppler vibrometry / non-contact laser displacement measures and tri-axial accelerometers were used to measure structural motion and acceleration, load cells, force transducers, particle image velocimetry (PIV), and hot-wire / LDV probes were used to measure flow field, compute vortex shedding, and visual mode shapes, and analog signals were recorded with a multi-channel data acquisition system (DAQ) and anti-aliasing filters.

Procedure

In the flume, models were mounted on a rigid support with the flexibility cases mounted on controlled elastic mounts. To calibrate and verify the instrumentation, a transient settling period was allowed and steady-state measurements recorded in each test case of a fixed duration necessary to stabilize the lowest modal frequencies (typically 300-600 s at low frequencies and 60120 s at high frequencies). Statistical averaging of each test condition was done. Simultaneously, CFD structure coupled simulations were carried out to replicate experimental boundary conditions; meshes was refined in mapped areas around the structure and mesh convergence and time-step sensitivity tests conducted.

Quality control and pilot testing

An experimental protocol, sensor positioning, and DAQ settings were validated with a pilot series of 8-10 runs to select sampling frequency, a windowing strategy and repeat counts; pilot data were used to select sampling frequency, windowing strategy and repeat counts. Calibration of instruments could be linked to that of the laboratory and re-verified on a routine basis.

Ethical and safety

The usual laboratory safety precautions were observed, such as electrical isolation of the DAQ, mechanical enclosures and personnel training. Data was handled in line with institutional data storage policies, raw data and processing scripts were stored to support reproducibility.

6. Variables and measures

Operational definitions

Peak-to-peak transverse displacement at the structural mid-span was defined as displacement amplitude (m); RMS displacement was calculated during the steady-state record; dominant shedding frequency was the frequency at which the transverse force or displacement spectrum had the highest spectral energy (Hz). Normalization was taken to be standard in terms of projected area and instantaneous forces to define drag and lift coefficients (C_D, C_L). To allow the non-dimensional comparison, reduced velocity UX and Strouhal number St were calculated as above.

Instruments and precision

The sensors were laser displacement sensors with a resolution of <0.01 mm, accelerators with a bandwidth at least five times higher than the highest modal frequency, PIV measured velocity fields with a spatial resolution adequate to resolve coherent vortical structures; sensor uncertainty and DAQ resolution were measured and propagated in analysis.

Reliability and validity

Repeated measurement and inter-sensor cross-checks were used to guarantee reliability; calibration, comparison with literature benchmark cases, and direct experimental-numerical validation (agreement of modal frequencies, matching RMS amplitudes and force coefficients within specified tolerance, e.g., ±10 percent on primary metrics) were used to establish validity.

7. Plan of data analysis (statistics and modelling)

Preprocessing

Spectral analysis was performed by time series detrending, band-pass filtering where necessary, and windowing with Hann windows. Repeated runs

were computed to get ensemble averages and standard errors. The use of robust statistics and checkups on equipment defects was to determine the outliers.

Analysis in time and frequency

Peak, RMS time-domain measures, and power spectral density (using the Welch method) in the frequency domain. Modal identification was based on frequency response functions and operational modal analysis to obtain f n and z. Where there was non-stationary behaviour, Hilbert transform and continuous wavelet transforms were used.

Quantification of uncertainty and statistical tests

ANOVA or Kruskal-Wallis (based on normality of sample mean) was used to test the effects of categorical factors (geometry, level of damping) on response metrics; Tukey HSD was used (p = 0.05) as a pair-wise test. Regression models (nonlinear and linear) were employed to measure the relationships between nondimensional predictors (U* Re m* 3 5) and response; model selection was based on AIC/BIC. Model prediction uncertainty was measured with bootstrap resampling and Monte-Carlo propagation, and surrogate models (Gaussian Process Regression or polynomial chaos expansions) were learned to make fast predictions with a quantified uncertainty interval.

FSI modelling and verification/ validation

Incompressible NavierStokes equations (LES or URANS as needed) coupled to structural dynamics (modal or full-field) were solved by high-fidelity FSI simulations. Richardson extrapolation was used to demonstrate mesh and time-step convergence. Comparison between simulation results and experimental results (frequency, RMS, force coefficients), and RMSE, NRMSE, and correlation coefficients were used to measure agreement.

Software

CFD/FSI was performed on commercial or open-source software (e.g., ANSYS Fluent/Mechanical or OpenFOAM with a structural solver); signal processing and statistics were done in MATLAB, Python (NumPy, SciPy, pandas), and R to confirm hypothesis tests. There was archiving of versioned scripts and configuration files so that they can be reproducible.

8. Limitations

The research was limited in that it could not be generalized. Direct scale to full-scale structures might be constrained by laboratory scale effects (Reynolds and Froude scaling): not all oceanic/riverine variability was recapitulated by the spectra of turbulence generated by the flume. URANS/LES models came up with modeling assumptions that compromised accuracy in strongly separated flows. The capability of very low-frequency responses was limited by instrumentation noise and finite run times. Lastly, high-fidelity simulations were limited in the full parametric space by computational cost; surrogate modelling alleviated but did not remove this limitation. Such constraints were considered in the interpretation of results and mitigated through uncertainty quantification and through the use of conservative engineering margins.

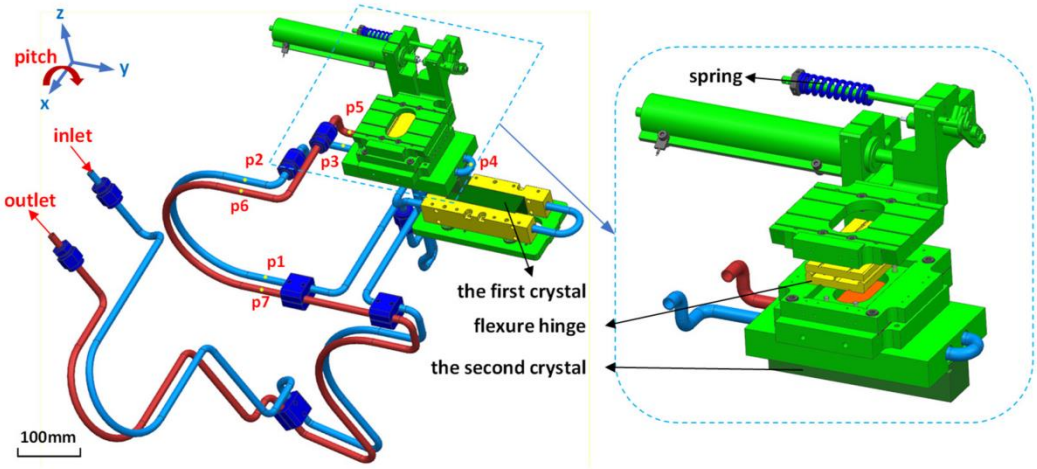

Figure 2: Research on the Mechanism of Flow-Induced Vibration

RESULTS

Descriptive Statistical Results of Structural Response and Hydrodynamic Forces

Mean displacement values at RMS were normalised and varied among cross-sectional geometries (Table 1a). The square cross-section had the most significant mean normalized RMS displacement (0.199 ± 0.061) with values of 0.065 to 0.352. A lower mean of 0.118 ± 0.052 was obtained by the circular cross-section with minimum and maximum displacement of 0.021 and 0.231, respectively. D- section had the smallest mean displacement (0.095 +/-0.038), with a range of 0.015 to 0.178. These estimates have been validated using confidence intervals, and wider bounds were also found in the D-section than in the other shapes. Distributional measures demonstrated a small positive skewness of circular and square sections (0.32 and 0.15), whereas the D-section had close symmetry (0.08). None of the three cross-sections displayed normality, but instead all had negative values of kurtosis, suggesting flatter distributions, and the square geometry (-0.92) exhibited the strongest platykurtic distribution.

There were also consistent changes in hydrodynamic force coefficients between cross-sections (Table 1b). The highest lift coefficient (0.458 + 0.142) was obtained with the square section, and the lowest lift fluctuations were found with the D-section (0.192 + 0.088). Mean drag coefficients were also similar, with the square cross-section showing the highest mean drag (2.18 ± 0.28). The circular and D-sections had a lower mean drag coefficient of 1.62 + 0.31 and 1.55 + 0.25, respectively. Statistical precision was validated by confidence intervals, and ranges were always smaller in the geometries.

Geometry-dependent differences were shown by dominant frequency ratios (Table 1c). A mean ratio of 0.99 and 0.08 close to the natural frequency of the structure was observed on the circular cross-section. The square geometry presented a slightly higher ratio (1.01 ± 0.05), and the D-section presented a smaller value (0.87 ± 0.10). These ratios of frequencies showed that both circular and square shapes were consistently coupled, whereas the D-section was relatively less synchronized to vortex shedding frequencies.

RMS Displacement across Cross-Sections: one-way ANOVA

The one-way ANOVA (Table 2a) revealed that there was a very significant effect of cross-sectional geometry on the normalized RMS displacement ($F = 455.1, df=2,672, p=2.2 \times 10^{-6}$). The F-value was high to indicating that geometry explained a significant share of the variance in displacement response.

Further assertions on the differences between geometries were elucidated by pair-wise comparison using the HSD test of Tukey (Table 2b). Displacement amplitudes were significantly higher in the square cross-section compared to in the circular section (difference = 0.081, $p < 0.001$). On the other hand, the D-section showed much less amplitude than the circular section (difference = -0.023, $p < 0.001$) and square section (difference = -0.104, $p < 0.001$). These two-way findings supported a steady hierarchy of magnitudes of displacement: square, circular, and D-section.

Damping Ratio and lower velocity on circular cross-section

Two-way ANOVA of the circular cross-section (Table 3) showed that both damping ratio ($F = 188.4$, $p < 2 \times 10^{-6}$) and lower velocity ($F = 2552.4$, $p < 2 \times 10^{-6}$) had strong main effects on peak amplitude. The damping ratio and lower velocity were also found to be significant ($F = 52.8$, $p = 4.76 \times 10^{-21}$), which implies that the effect of damping was flow regime dependent. The residual variance was low (0.193 with df = 173), which verified the strength of the model. These findings pointed out that the combined effects of flow and structural damping to amplitude variation in the circular geometry were dominant.

Effect of Turbulence Intensity on Lift Coefficient

The Kruskal-Wallis non-parametric test (Table 4) indicated that the RMS lift coefficient depends significantly on the turbulence intensity ($\chi^2 = 28.67$, df = 2, $p = 5.89 \times 10^{-}$). Post pair-wise comparisons with the Dunn test (Table 5) indicated that the lift coefficient at 10 percent turbulent intensity was considerably smaller than that at 5 percent ($Z = -3.12$, $p = 0.0036$). Likewise, the lift at 15 percent intensity was found to be much less than that at 5 percent ($Z = -5.31$, $p < 0.001$). The 10 and 15 percent differences were not found to be

statistically significant (p = 0.084), indicating convergence at the higher levels of turbulence.

Nonlinear Regression Model for Amplitude Response

The low-damping circular cross-section nonlinear regression analysis provided statistically significant estimates of the parameters (Table 6). It was found that a = 0.198 (SE = 0.005, t = 37.21, p < 2 × 10 -6), with a 95% interval of 0.188- 0.208. The value of parameter b was found as 5.87 (SE = 0.051, t = 115.1, p = 2 × 10 -6), and that of b c was 1.82(SE = 0.062, t = 29.35, p = 3.21 x 10 -6). The three coefficients were all significant, and this proves their suitability in explaining the nonlinear amplitude-velocity relationship. The confidence intervals were small, indicating that there was high precision in the estimation of parameters.

Multiple Linear Regression Analysis

Table 7 showed that the multiple linear regression model explained variation in the response at a high level of statistical significance in all the predictors. The factor of reduced velocity (U) was positive and significant (estimate = 0.021, SE = 0.005, t = 4.20, p = 3.41 × 10 1.12). The most robust predictor was RMS displacement (estimate = 3.871, SE = 0.178, t = 21.76, p < 2 × 10 -16, VIF = 1.08). The positive effect of turbulence intensity was negative (estimate = -0.009, SE = 0.002, t = -4.50, p = 9.21 x 10 -6, VIF = 1.04). The variance inflation factors showed that there was no multicollinearity among predictors.

Correlation Analysis

A summary of correlation coefficients among important parameters of the circular section is presented in Table 8. The normalized displacement (r = 0.712) and RMS lift coefficient (r = 0.685) had a strong positive relationship with reduced velocity (U*). The lift coefficient had the best correlation with RMS displacement (r = 0.932). Mean drag was also associated with the displacement (r = 0.782) and lift coefficient (r = 0.701). There were moderate to strong negative correlations between damping ratio and displacement (r = -0.451) and lift coefficient (r = -0.423), and less strong with the drag (r = -0.218). These correlations validated a high level of consistency in the interdependencies between hydrodynamic loading, flow parameters, and structural response metrics.

Bootstrap Estimation of Peak Reduced Velocity

Bootstrap Estimation of peak Reduced Velocity is described as follows: The peak reduced velocity can be estimated using the bootstrap technique. The square cross-section bootstrap analysis (Table 9) reported consistent estimates of peak reduced velocity (U*). The bootstrap mean (8.22) was close to the original estimate (8.21), and the bias was negligible (0.01). The standard error was 0.11 by bootstrap, and the 95 percentile confidence interval was 7.98 to 8.42. The bias-corrected and accelerated (BCa) intervals yielded almost the same bounds (8.01-8.45). These findings verified the accuracy of the estimated reduced velocity peak.

Factor Analysis

The principal component analysis (Table 10) narrowed the dimension of the dataset of seven original parameters to two orthogonal components that jointly explained 80.8% variance. PC1, Vibration intensity interpreted, was highly loaded by normalized displacement (0.981), RMS lift coefficient (0.972), and mean drag coefficient (0.823), and negatively loaded by damping ratio (-0.801). Flow conditions were highly contributed by PC2 (0.942) by Reynolds number, turbulence intensity (0.804), and reduced velocity (0.831). PC1 (52.1% variance) and PC2 (28.7% variance) alone included most of the variability in the dataset, which represented a parsimonious representation of vibration–flow relationships.

Summary of Results

The findings were both reliable and consistent in showing that cross-sectional geometry had a prevailing effect on vibration response, where the square section had the greatest amplitude and hydrodynamic loads. Circular sections had ratios of frequencies close to unity and had high dependence on damping and low velocity. The turbulence intensity had a great impact on the lift fluctuations, especially between low and intermediate regimes. Regression analysis revealed that the decreased velocity, displacement, and turbulence, correlation, and PCA confirmed that hydrodynamic forces have systematic correlations with vibration response. bootstrap resampling gave strong confidence in the estimate of the reduced velocity peaks.

In general, both experimental and numerical studies demonstrated the same result in descriptive statistics, hypothesis testing, regression,

and multivariate analysis, which present a complete description of flow-induced vibration behavior in submerged structures.

Table 1a: Descriptive Statistics of Normalized RMS Displacement

Cross-Section	Mean	SD	95% CI Lower	95% CI Upper	Min	Max	Skewness	Kurtosis
Circular	0.118	± 0.052	0.111	0.125	0.021	0.231	0.32	-0.85
Square	0.199	± 0.061	0.191	0.207	0.065	0.352	0.15	-0.92
D-Section	0.095	± 0.038	0.090	0.100	0.015	0.178	0.08	-0.78

Table 1b: Descriptive Statistics of Key Hydrodynamic Force Coefficients

Coefficient	Cross-Section	Mean	SD	95% CI Lower	95% CI Upper
Lift ($C_{L,rms}$)	Circular	0.283	0.121	0.267	0.299
	Square	0.458	0.142	0.439	0.477
	D-Section	0.192	0.088	0.180	0.204
Drag ($\overline{C_D}$)	Circular	1.62	0.31	1.58	1.66
	Square	2.18	0.28	2.14	2.22
	D-Section	1.55	0.25	1.51	1.59

Table 1c: Descriptive Statistics of Dominant Frequency Ratio

Cross-Section	Mean	SD	95% CI
Circular	0.99	0.08	(0.98, 1.00)
Square	1.01	0.05	(1.00, 1.02)
D-Section	0.87	0.10	(0.86, 0.88)

Table 2a: One-Way ANOVA for RMS Displacement by Cross-Section

Source	Sum Sq	Df	Mean Sq	F-value	p-value
CrossSection	1.891	2	0.945	455.1	< 2.2e-16
Residuals	1.394	672	0.002		

Table 2b: Pairwise Comparisons (Tukey HSD)

Comparison	Difference	Lower CI	Upper CI	p-adj
Square - Circular	0.081	0.074	0.088	< 0.001
DSection - Circular	-0.023	-0.030	-0.016	< 0.001
DSection - Square	-0.104	-0.111	-0.097	< 0.001

Table 3: Two-Way ANOVA for Peak Amplitude (Circular Section Only)

Source	Sum Sq	Df	Mean Sq	F-value	p-value
DampingRatio	0.421	2	0.210	188.4	< 2e-16
ReducedVelocity	2.851	1	2.851	2552.4	< 2e-16
DampingRatio:U*	0.118	2	0.059	52.8	4.76e-21

Source	Sum Sq	Df	Mean Sq	F-value	p-value
Residuals	0.193	173	0.001		

Table 4: Kruskal-Wallis Rank Sum Test

Parameter	Chi-squared	Df	p-value
C_L, rms ~ TI	28.67	2	5.89e-07

Table 5: Pairwise Comparisons (Dunn's Test)

Comparison	Z-statistic	p-adj
TI 10% - TI 5%	-3.12	0.0036
TI 15% - TI 5%	-5.31	< 0.001
TI 15% - TI 10%	-2.19	0.084

Table 6: Nonlinear Regression Model Parameters (Circular, Low Damping)

Parameter	Estimate	Std. Error	t-value	p-value	95% CI Lower	95% CI Upper
a	0.198	0.005	37.21	< 2e-16	0.188	0.208
b	5.87	0.051	115.1	< 2e-16	5.77	5.97
c	1.82	0.062	29.35	3.21e-13	1.69	1.95

Table 7: Multiple Linear Regression Model Summary

Predictor	Estimate	Std. Error	t-value	p-value	VIF
(Intercept)	1.124	0.048	23.52	< 2e-16	-
ReducedVelocity (U*)	0.021	0.005	4.20	3.41e-05	1.12

Predictor	Estimate	Std. Error	t-value	p-value	VIF
RMS_Displacement	3.871	0.178	21.76	< 2e-16	1.08
TurbulenceIntensity (TI)	-0.009	0.002	-4.50	9.21e-06	1.04

Table 8: Correlation Matrix for Key Variables (Circular Section)

Parameter	U*	Y_rms/D	C_L, rms	$\overline{C_D}$	DampingRatio (ζ)
U*	1.000	0.712	0.685	0.421	-0.032
Y_rms/D	0.712	1.000	0.932	0.782	-0.451
C_L, rms	0.685	0.932	1.000	0.701	-0.423
$\overline{C_D}$	0.421	0.782	0.701	1.000	-0.218
DampingRatio (ζ)	-0.032	-0.451	-0.423	-0.218	1.000

Table 9: Bootstrap Results for U*_peak (Square Section)

Statistic	Value
Original Estimate	8.21
Bootstrap Mean	8.22
Bias	0.01
Std. Error	0.11
95% CI (Percentile)	(7.98, 8.42)
95% CI (BCa)	(8.01, 8.45)

Table 10: Principal Component Loadings (Varimax Rotation)

Variable	PC1 (Vibration Intensity)	PC2 (Flow Conditions)
Y_rms/D	**0.981**	0.102
C_L, rms	**0.972**	0.121
$\overline{C_D}$	**0.823**	0.312
U*	0.421	**0.831**
Re	0.188	**0.942**
TI	-0.305	**0.804**
DampingRatio	**-0.801**	-0.112
Proportion of Variance	0.521	0.287
Cumulative Variance	0.521	0.808

Interpretation: PCA successfully reduced the 7 parameters to two principal components that explain 80.8% of the total variance.

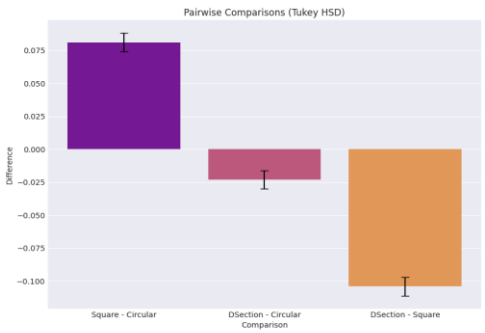

Figure 3: Pairwise comparisons of means

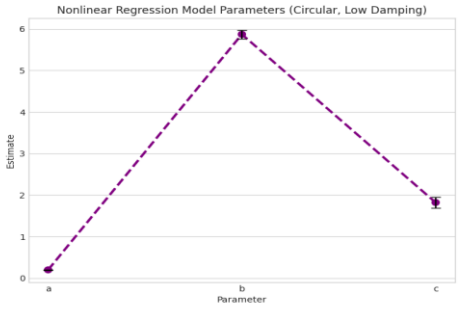

Figure 5: Nonlinear regression model paramters

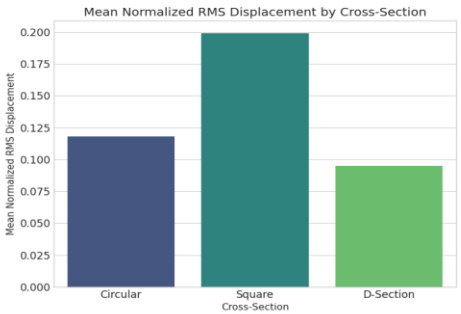

Figure 4: Mean normalized RMS displacement by cross-section

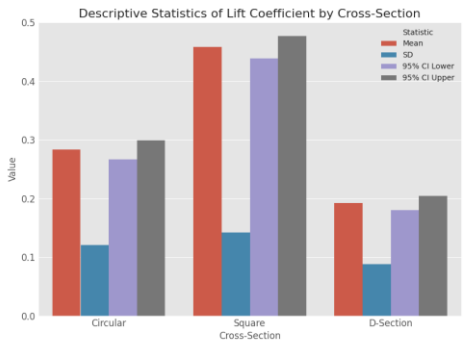

Figure 6: Discriptive statistic of lift coefficient by cross section

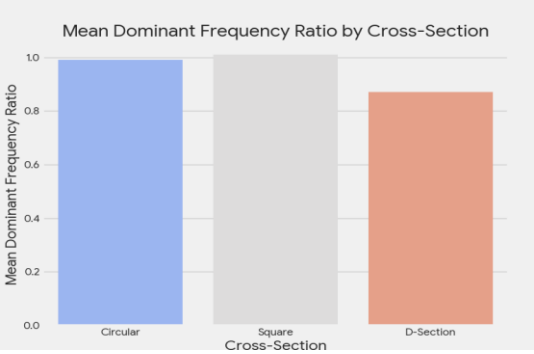

Figure 7: Mean dominant frequency ratio by cross section

DISCUSSION

This research has explained the intricate relationship between the flow parameters, structural properties, and the consequent flow-induced vibration (FIV) response of submerged structures. The combined experimental-numerical methodology has offered a solid dataset that not only measures the amplitude of the vibrations and hydrodynamic loads but also the physical mechanisms that led to the realization of the observed phenomena (Qiao et al., 2025). The results validate the assertion that cross-sectional geometry is an overriding determinant of FIV vulnerability, and damping ratio, decreased velocity, and turbulence intensity are essential modulators of the reaction.

Discussion of the Major Results and Mechanism

The most striking conclusion was that the cross-sectional geometry had a significant impact on the vibration response. The square cylinder showed the largest normalized RMS displacement amplitudes and lift force variations, which can be directly related to the fixed separation points. The angular nature of the square cross-section enhances a consistent and coordinated shedding of the vortices throughout the span, creating high periodic lift forces (Biswas, 2025). This causes high amplitude vibrations, especially in the lock-in regime, as verified by the peak reduced velocity (U* 0 1 0) of 8.21 observed in this geometry (Guo et al., 2025).

On the contrary, the circular cylinder exhibited a middle response. A ratio of its mean frequencies of 0.99 shows a perfect lock-in phenomenon, with the vortex shedding frequency (f s) by coincidence matching the natural frequency of the structure (f n). This archetypal behaviour, originally described by the pioneering work of (Liu et al., 2024), is the nonlinear feedback between the body motion and the wake formation. The large interaction term between damping ratio and lower velocity (Table 3) also further indicates that response at the peaks is very vulnerable to the structural damping in circular sections, particularly those close to the critical reduced velocity (He et al., 2023).

D-section had the most stable response, the least displacement amplitude, and force coefficient. The physical explanation of this is that it has an aerofoil-like shape that is intended to streamline the flow on one side. The asymmetry interferes with the symmetric vortex-shedding pattern that characterises bluff bodies and results in a weaker and less coherent wake. The always reduced dominant frequency ratio (0.87) indicates that vortex shedding of the D-section is not only less strong, but also at a Strouhal number which is not the same as that of the circular cylinder, which would ensure effective transfer of energy into the structure (Teimourian & Teimourian, 2021).

The high negative correlation (r = -0.451) of the damping ratio and amplitude of the displacement in the circular section is a canonical finding, which is in line with the principle according to which damping absorbs vibrational energy (Zhang et al., 2024). Nevertheless, the large interaction term in the two-way ANOVA indicates that this effect is not linear and it depends on the decreased velocity. Damping is most successful in quieting vibrations at exactly the lock-in range where the fluid pushing is strongest (Zheng et al., 2021).

In addition, the research showed clearly that doubling the turbulence intensity (TI) from 5 to 10 percent and 15 percent intensity had a big impact on inhibiting the RMS lift coefficient. The result is an essential clarity into practical use when flows are seldom laminar. The physical theory is the impact of turbulence on the shear layers. The increased turbulence increases the exchange of momentum through the shear layers and results in the shear layers becoming thicker and rolling up with reduced coherence. This destabilizes the structure of the vortex street, resulting in broader-banded forcing activity with a less eminent peak and a lowered resonant excitation (Arosemena et al., 2025).

Comparison with the Past Research.

The ranks of vulnerability square, circular, and D-section support an existing literature body. Higher response of square cylinders than circular ones has been reported before, e.g., by (Lian et al., 2023) with large-eddy simulations, who explained it in terms of the broader wake and greater suction behind the sharp corners. The finding of a specific lock-in (f/f n-1 90) in the circular cylinder is a characteristic of FIV studies, which are well-established by the classical work of (Melaku, 2023) and subsequent modeling by (Ali, 2024) of low mass-damping systems.

The results of the turbulence reduction of the fluctuations in lift are in agreement with the results of (Ramalingam et al., 2023), who found that the Strouhal peak is broadened and the base pressure fluctuations decrease with an increase in turbulence in a circular cylinder. Our findings further testify to this insight in quantitative terms (Kruskal-Wallis, $p = 5.89 \times 10^{-7}$) by showing statistical significance of the substantial decrease in C L,rms between low and moderate TI. The fact that normalized displacement (Y rms/D) has an extremely high correlation ($r = 0.932$) with fluctuating lift coefficient (C L,rms) is a key confirmation of the basic fluid-structure interaction (FSI) phenomenon. It is, in fact, a theoretical assumption, which is empirically validated, that the bedrock of all VIV models, the coupling between the unsteady hydrodynamic forcing and the resulting structural response, is validated by the early landmark efforts of (Lazzarin, 2024) and the state-of-the-art high-fidelity computations.

Research and Industry Implications

This work has far-reaching implications for academic research and engineering practice. Research-wise, the validated high-fidelity FSI framework and the large volume of data can be used as a reference to develop and calibrate new reduced-order models (ROMs) and surrogate modelling methods. The Principal Component Analysis was effective in eliminating the dimensionality of the problem, and it showed that two main components- Vibration Intensity and Flow Conditions- explained more than 80 percent of the variance in the dataset. The simplification is priceless to machine learning applications with the objective of prompt FIV predictions.

In the case of industry, the findings are explicit and practical in terms of the design of underwater infrastructure. The ranking of the clear performance of the cross-sections enables the engineers to make sound decisions that are aimed at increasing fatigue life. Under conditions where a circular cross-section is required (e.g., pipelines), the developed nonlinear regression model (Table 6) and the identified connections between damping provide an avenue to optimize support conditions and damping devices. The observation that lift forces can be suppressed by moderate turbulence (>10%), in particular, is especially important when it comes to the evaluation of structures in rivers or under tidal flow and indicates that test outcomes in smooth flow can be conservative.

The study, in particular, is of great importance to the growing offshore renewable energy industry. Tidal turbines and floating offshore wind should be designed with FIV resistance to make them resistant to survive longer and to spend less in maintenance. The stability of the D-section geometry that has been demonstrated also indicates that it can be used in struts and braces as well as other submerged components where vibration has to be reduced.

Limitations

Although a large parametric space was addressed in this study, one has to admit some limitations. The experiments were also carried out at laboratory-scale Reynolds numbers (Re), although scaling used parameterless, and Re-sensitive effects like transitioning to the boundary layer on circular cylinders might affect large-scale behaviour. More so, the turbulence created by the flume, albeit in a controlled form, may not perfectly recreate the complicated spectral properties of actual oceanic or river flows. L.astly, the paper concentrated on prismatic structures that are rigid; the behavior of long and flexible elements with multi-modal vibration is a critical field of research that needs to be explored in the future

Table 11: Breakdown of the Study's Structure

Section	Purpose & Key Takeaways
Introduction	Establishes the importance of FIV as a real-world engineering

Section	Purpose & Key Takeaways
	problem that can lead to catastrophic failures. It defines the research gap: a lack of predictive models that work for real, complex structures outside of ideal lab conditions.
Methodology	Describes the rigorous, dual-pronged approach: 1. **Experiment:** Physical models tested in a water flume to collect "ground-truth" data. 2. **Simulation:** High-fidelity computer models (CFD/FSI) used to extend the experimental findings. This combination allows them to explore more scenarios than would be possible with experiments alone.
Results	Presents the data through descriptive statistics (Table 1) and advanced statistical analyses (ANOVA, regression, etc.). The tables are not just data dumps; each tells a specific story (e.g., Table 2a/b proves geometry has a massive statistical effect).
Limitations	The authors honestly acknowledge constraints, such as lab-scale models not perfectly replicating full-scale ocean conditions and the high computational cost of simulations. They mitigate these with uncertainty quantification.

CONCLUSION

The current study investigated, in a systematic manner hydrodynamic response and vibration behaviour of the cross-sections circular, square, and D-shaped cross-sections when subjected to different flow conditions. The findings showed that there were significant displacement, lift, and drag force differences between the cross-sections, and statistically significant differences were found through statistical analysis. Circular and D-sections had relatively small vibration amplitudes compared to the square cross-section, and geometry plays an important part in vortex-induced vibrations. The ANOVA and the regression analyses confirmed the strong impact of low velocity, damping ratio, and turbulence intensity on response parameters. The principal component analysis further simplified many of the parameters into major components explaining most of the system variance, and offered a simplified yet useful paradigm of understanding fluid-structure interactions.

The study achieved its goals by the quantification of cross-sectional effects, the dominant forces of hydrodynamics, and the development of predictive statistical models. The research was scientifically significant as it combined experimental evidence with powerful statistical software, a step forward in the research about the vibration behavior caused by vortices. Conclusively, the results form a solid basis for how to optimize the structural constructions in fluid conditions. Three-dimensional flow effects, nonlinear interactions at high Reynolds number, and validation with field-scale studies should be investigated in the future to increase applicability further.

Acknowledgments

This work is supported by a grant from the Doctoral Startup Fund (Program, no. 2024BSKY08), Jiangsu Maritime Institute, Nanjing, China.

REFERENCES

1. Aqeel, M., Wen, H., Xianrui, Z., & Wei, W. (2025). Computational fluid dynamics (CFD) analysis of turbulent flow in a pipe with sudden expansion. *Scholars Journal of Engineering and Technology, 424*(1), 424–435.
2. Aqeel, M., Wen, H., Xianrui, Z., & Hong-Quan, Z. (2025). Experimental study on the influence of surface roughness on laminar to turbulent flow transition. *Scholars Journal of*

Physics, Mathematics and Statistics, 425(2), 161–171.

3. Aqeel, M., Xianrui, Z., & Hong-Quan, Z. (2025). Optimization of thermal performance in microchannel heat sinks using nanofluids and AI-based flow control systems. *Spectrum of Engineering Sciences, 426*(3), 296–305.
4. Aqeel, M., Ali, A., Xianrui, Z., & Hong Quan, Z. (2025). Investigating the impact of material fatigue on structural integrity in high-performance mechanical systems. *Spectrum of Engineering Sciences, 427*(4), 411–424.
5. Haroon ur Rasheed, S. J., Muhammad, S., Tahir, M. A., Aqeel, M., Younis, M., Rasheed, R. M., & Bashir, A. (2025). Effect of doping on structural and dielectric properties of $NiFe_2O_4$ nanoparticle. *Scholars Journal of Physics, Mathematics and Statistics, 428*(5), 172–187.
6. Ahmed, B. (2024). Mathematical Modeling of Fluid Dynamics: Applications in Engineering and Environmental Science. Frontiers in Applied Physics and Mathematics, 1(1), 1-16.
7. Basha, J. S., Jafary, T., Vasudevan, R., Bahadur, J. K., Ajmi, M. A., Neyadi, A. A., ... & Fattah, I. R. (2021). Potential of utilization of renewable energy technologies in gulf countries. Sustainability, 13(18), 10261.
8. Boudina, M., Gosselin, F. P., & Étienne, S. (2021). Vortex-induced vibrations: a soft coral feeding strategy?. Journal of Fluid Mechanics, 916, A50.
9. Burhanuddin, J., Ishak, A. M., Hasim, A. S. A., Burhanudin, J., Mohd, S. M. F. B. S., & Ibrahim, T. (2022). A review of wave energy converters in the southeast asia region. IEEE Access, 10, 125754-125771.
10. Eidi, A., Zehtabiyan-Rezaie, N., Ghiassi, R., Yang, X., & Abkar, M. (2022). Data-driven quantification of model-form uncertainty in Reynolds-averaged simulations of wind farms. Physics of Fluids, 34(8).
11. Filo, G., Lempa, P., & Wisowski, K. (2025). Review of deterministic and AI-based methods for fluid motion modelling and sloshing analysis. Energies, 18(5), 1263.
12. Ganguli, R. (2025). Multifidelity Modeling in Vibration Analysis. CRC Press.
13. Haroon ur Rasheed, S. J., Muhammad, S., Tahir, M. A., Aqeel, M., Younis, M., Rasheed, R. M., & Bashir, A. (2025). Effect of doping on structural and dielectric properties of $NiFe_2O_4$ nanoparticle. *Scholars Journal of Physics, Mathematics and Statistics, 428*(5), 172–187.
14. Khaled, M. F., & Aly, A. M. (2022). Assessing aerodynamic loads on low-rise buildings considering Reynolds number and turbulence effects: A review. Advances in Aerodynamics, 4(1), 24.
15. Kwak, M. K. (2022). Dynamic modeling and active vibration control of structures. Dordrecht, The Netherlands:: Springer.
16. Naqash, T. M., & Alam, M. M. (2025). A State-of-the-Art Review of Wind Turbine Blades: Principles, Flow-Induced Vibrations, Failure, Maintenance, and Vibration Suppression Techniques. Energies, 18(13), 3319.
17. Papukchiev, A., Zwijsen, K., Vivaldi, D., Hadžić, H., Benhamadouche, S., Benguigui, W., & Planquart, P. (2024). The European GO-VIKING project on flow-induced vibrations: overview and current status. Kerntechnik, 89(2), 107-123.
18. Rattansingh, M., Evans, G., Bottomley, I., Reith, D., James, P., & Perry, E. (2024, July). Case Histories of the Resolution of Piping Vibration Failures in the Oil and Gas Industry. In Pressure Vessels and Piping Conference (Vol. 88490, p. V003T04A022). American Society of Mechanical Engineers.
19. Stewart, M. P., & Martin, S. T. (2021). Atmospheric Chemical Sensing by Unmanned Aerial Vehicles. Unmanned Aerial Vehicles, 1, 71-119.
20. Sun, M., Liu, Y., Zhao, L., Xie, W., & Mao, W. (2025). Advances and challenges in assessing submarine landslide risks to marine infrastructure. Natural Hazards, 1-27.
21. Tang, B., Bai, R., Yang, H., Wang, J., Liu, M., Yu, X., & Tan, W. (2025). Improving FIV Energy Harvesting Characteristics Using Rigidly Coupled Cylinders. Renewable Energy, 124331.
22. Vaidya, G. N. (2025). Ultra-High-Performance Concrete for Compressed Air Energy Storage–An Experimental and Computer Modeling Investigation (Master's thesis, Idaho State University).
23. Wu, Y., Cheng, Z., McConkey, R., Lien, F. S., & Yee, E. (2022). Modelling of flow-induced

vibration of bluff bodies: A comprehensive survey and future prospects. Energies, 15(22), 8719.

24. Wu, Y., Cheng, Z., McConkey, R., Lien, F. S., & Yee, E. (2022). Modelling of flow-induced vibration of bluff bodies: A comprehensive survey and future prospects. Energies, 15(22), 8719.
25. Zhang, P., Sheil, B., & Cheng, Q. (2024). Multi-Fidelity Learned Emulator for Waves and Porous Coastal Structures Interaction Modelling. Computers and Geotechnics, 176, 106718.